Forced Oscillation Experiments in Supercritical Diffuser Flows

M. Sajben,* T. J. Bogar,† and J. C. Kroutil‡
McDonnell Douglas Corporation, St. Louis, Missouri

Low-frequency oscillations induced in ramjet inlets by combustion instabilities were simulated by mechanically modulating the exit area of a two-dimensional, supercritical diffuser at frequencies up to 330 Hz. Boundary layers were attached below a terminal shock Mach number of 1.27, and shock-induced separation occurred above this value up to the experimental limit of 1.35. Shock position histories were obtained and streamwise distributions of static/total dynamic pressures were determined both on the wall and within the flow for various shock strengths and frequencies. Excitation at the natural frequencies of the shock motion produced no obvious resonance effects. For weak shocks, the perturbations and their reflections from the shock are reasonably approximated by one-dimensional, acoustic considerations, but this description fails for strong shocks.

Nomenclature

a = speed of sound
A = admittance ratio (defined in Appendix)
f = frequency
h = channel height
i = $\sqrt{-1}$
M = Mach number
p,P = pressure and Fourier coefficient of pressure, respectively
R = reflection coefficient
t = time
u,U = velocity and Fourier coefficient of velocity, respectively
x = streamwise coordinate ($x=0$ at throat, positive streamwise
y = vertical coordinate ($y=0$ on bottom wall, positive upwards)
α = perturbation phase
γ = ratio of specific heats, $=1.4$
ν_e = pressure ratio, $=p_{t0}/P_{se}$
ρ = density
ϕ_P = phase angle for pressure
ϕ_U = phase angle for velocity
ψ = argument of complex reflection coefficient

Subscripts

e = exit station
n = order of Fourier harmonic
m = midstream ($\tilde{y}=0.432$, core probe or line-scan camera scanning height)
s = static
t = total
u = upper wall
0 = plenum chamber
$()_*$ = throat
σ = shock
$\bar{()}$ = ensemble average
$\underset{\sim}{()}$ = time-dependent component of ensemble average

Superscripts

$\bar{()}$ = time-mean component
$()'$ = time-dependent component
$\hat{()}$ = rms of time-dependent component
$\tilde{()}$ = length normalized by throat height ($=h_*=44.1$ mm); also, pressure or velocity normalized according to Eq. (A5)

Received Sept. 24, 1982; revision received July 11, 1983.

*Principal Scientist, McDonnell Douglas Research Laboratories. Associate Fellow AIAA.

†Scientist, McDonnell Douglas Research Laboratories. Senior Member AIAA.

‡Unit Chief, Laboratory, McDonnell Douglas Research Laboratories. Member AIAA.

Introduction

INTEGRAL rocket/ramjet propulsion systems under development for use in future missiles have shown a tendency to exhibit undesirable pressure fluctuations. The fluctuations are most likely to occur in dump combustor systems in which an abrupt enlargement of cross section occurs at the inlet/combustor interface. The oscillations cover a wide range of frequencies; however, the low-frequency (below 500 Hz) range is the most troublesome region because of the possibility of inducing longitudinal oscillations in the inlet flow. The amplitudes may be large (20% of the mean combustor static pressure) and may cause expulsion of the terminal shock system from the (usually supercritical) inlet, thereby leading to an unacceptable reduction of inlet mass flow and loss of thrust.

This phenomenon was investigated in an ad hoc fashion during several development projects; the first studies explicitly concerned with dump combustor pressure oscillations were conducted byRogers[1,2] and Clark.[3] A simple theoretical framework for the description of the oscillations was formulated by Culick and Rogers,[4,5] using a small-perturbation (acoustic) analysis.

The present study explores the role of the inlet in pressure oscillations by experimentally investigating an idealized system that contains the essential elements of the ramjet inlet flow. The experiment represents the inlet by a two-dimensional, supercritically operated diffuser in a direct-connect mode (Fig. 1). The flowfield contains a terminal-shock/boundary-layer interaction region which may or may not exhibit separation of the top-wall boundary layer.[6-8] Two-dimensionality of the flow allows the use of powerful optical techniques (high-speed schlieren photography, laser velocimetry, and electronic imaging techniques), permitting the acquisition of information not accessible in three-dimensional configurations. Two-dimensionality also helps in reducing the complexity of the problem to a level amenable to theoretical treatment.[9-10]

Combustor pressure oscillations are simulated by mechanical modulation of the diffuser cross-sectional area

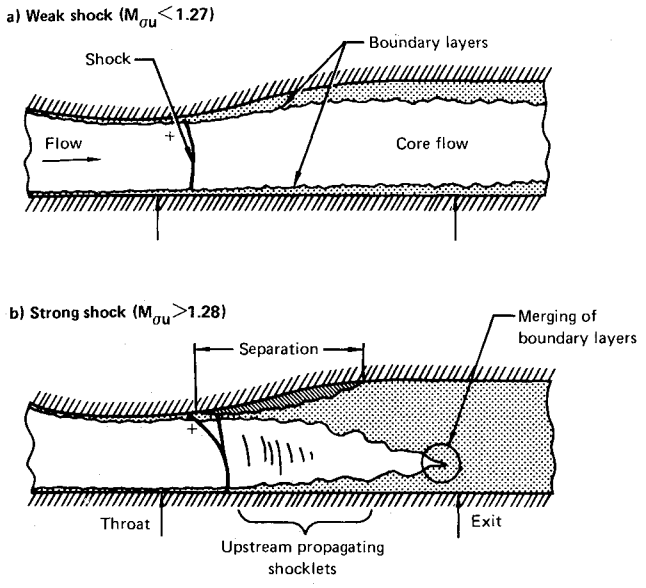

Fig. 1 Flow patterns observed in supercritical diffuser flows. M_{ou} is Mach number at plus signs. Vertical scale doubled.

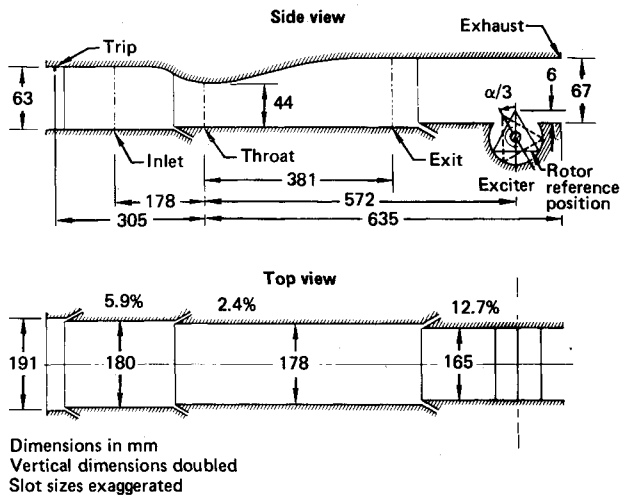

Fig. 2 Schematic of diffuser model.

near the channel exhaust. In operational ramjet systems, the diffuser flow oscillations feed back into the combustor, and a close coupling between the two is possible. Such a coupling is not simulated in the present experiment, which is a study of the diffuser response to an externally imposed downstream perturbation that is independent of the response it evokes.

The diffuser investigated here has been studied in detail earlier; both the time-mean flow and the naturally present fluctuations have been explored and documented.[11] Detailed laser Doppler velocimeter (LDV) flowfield measurements also are available for both natural and forced oscillations.[12] Additional details of the experiment and the time-mean flow can be found in Refs. 11-14.

Experimental Apparatus and Procedures

Diffuser Model

Figure 2 illustrates that the diffuser model is a convergent-divergent channel with initial and terminal constant-area segments. The minimum channel height (throat) is 44.1 mm, the width-to-height (aspect) ratio of the throat cross section is 4.0, and the exit-to-throat area ratio is 1.52. The top wall is contoured to produce boundary layers that are attached everywhere at fully subsonic and moderately supercritical conditions. Contour coordinates are given in Ref. 11. Sidewall boundary-layer growth was limited by the slot system through which approximately 20% of the initial flow was removed. Two-dimensionality of the flow was excellent with attached flow and acceptable with flow separation.[11] Most of the contoured channel segment is bounded on its sides by schlieren-quality windows, permitting optical access to the region of primary interest.

Nominal inlet and exit stations were chosen to lie within the constant-area segments and were instrumented to establish the initial and final flow states.

Excitation of the flow was accomplished by rotating a triangular, prism-shaped rotor partially embedded in the bottom wall and driven by a variable-speed motor about a spanwise axis. Shaft frequency could be varied continuously from 5 to 110 Hz, corresponding to excitation frequencies of 15-330 Hz. Rotor speed was held constant within ±1%. An optical encoder mounted on the rotor shaft produced 360 pulses per revolution (120 pulses per oscillation cycle), which were used in data acquisition and reduction to synchronize sampling and averaging operations. A photograph of the model installed in a flow facility is given in Fig. 3.

Instrumentation and Data Reduction

Twenty time-mean flow properties were monitored and recorded routinely throughout the test series, including pressures, temperatures, primary flow rate, individual bleed flow rates through each slot, mean and rms values of shock position, and mean and rms values of surface pressure fluctuations at selected locations. Time-mean wall pressure distributions were determined by numerous wall static orifices for all operating conditions of significance using a 96-channel Scanivalve system.

Fluctuating wall-surface pressures were measured by high-response transducers at seven streamwise positions on the top wall. One of these stations, the exit, was equipped with four transducers, two on the top wall and two on the bottom wall.

Two diagnostic methods were of particular importance to this study. An optical technique employing a line-scan camera was used to generate an instantaneous shock-position signal,[15,16] and a dual-pressure probe[13] was used to detect instantaneous total and static pressures within the core flow. The probe was mounted in a traverse gear embedded in the lower diffuser wall to allow the probe to be positioned in the streamwise direction from $\tilde{x}=0$ to 8. The sensing elements were miniature pressure transducers mounted in 3.2-mm-diam cylinders aligned with the flow. The two cylinders were 12.7 cm apart and 19 mm above the flat bottom wall. The (unmounted) natural frequency of the transducers was 500 kHz. The probe did not appreciably alter the wall static-pressure distributions nor influence the overall integral performance parameters (such as mass flow ratio or pressure recovery) unless it was located sufficiently close to the shock to pierce it intermittently.

Four types of dynamic data were recorded: shock position, top-wall static pressures, core-probe static pressure, and core-probe total pressure. All signals were recorded on tape using a 14-channel FM tape recorder (Sangamo Sabre III) and were subsequently processed in the following manner.

The analog data were digitized at 20 kHz for a period corresponding to 150 oscillation cycles. The data for each cycle were replaced by a set of 360 interpolated points corresponding to constant, 1 deg increments of α, as opposed to constant increments of time used in the digitizing procedure. This interpolation compensated for minor fluctuations in the exciter angular speed. The α value assigned to each data sample was calculated at $360tf$ (deg), where t is the time between the latest reference pulse and the instant of acquiring the sample and f is the excitation frequency. One reference pulse per excitation cycle was generated (using the shaft-mounted encoder signal and suitable circuitry) at the

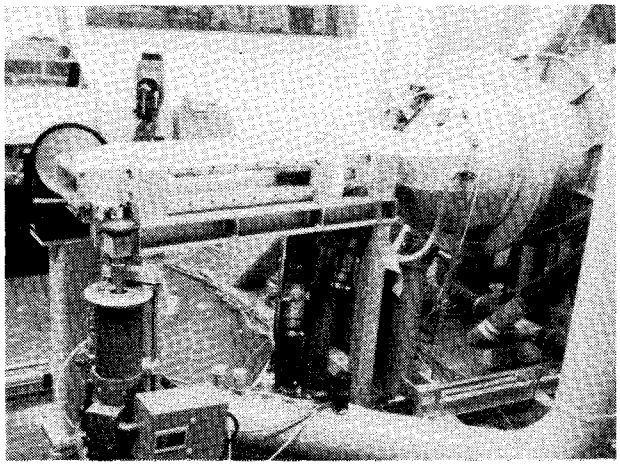

Fig. 3 Diffuser model installed in test facility. Components of schlieren system visible in background. Exciter drive motor and gear at left. Large-diameter pipe at bottom connects boundary-layer control slots to vacuum pump.

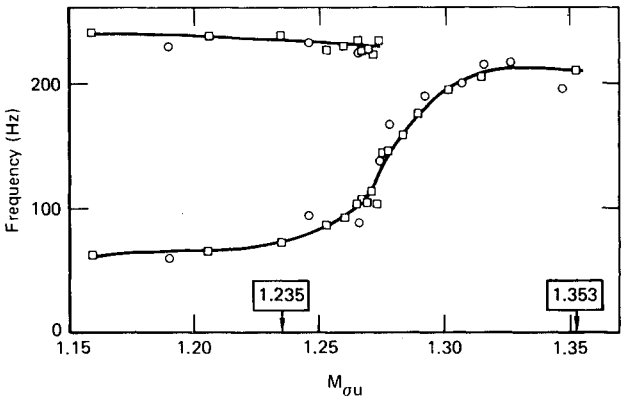

Fig. 4 Mach number dependence of shock motion spectral peaks. Framed numbers indicate conditions selected for detailed study with excitation.

instant of minimum cross-sectional area at the exciter, i.e., when a vertex of the rotor was located directly above the rotor axis (Fig. 2).

The interpolated data were averaged over 150 oscillation cycles to provide, as functions of α, the ensemble-averaged signal and the standard deviation of the 150 samples. The average of the standard deviations over one cycle was also computed as a measure of the time-mean contribution of the random fluctuations to the signal.

The ensemble-averaged waveforms were next Fourier-analyzed, retaining the first five harmonics, which resulted in the following form of decomposition for all dynamic data:

$$\underset{\sim}{y}(\alpha)=\bar{y}+\underline{y}(\alpha)\simeq\bar{y}+\sum_{n=1}^{5}Y_n\cos(n\alpha-\phi_n) \qquad (1)$$

where y can signify any of the signals. The variable α is the perturbation phase and should be distinguished from the phase angle associated with the various Fourier harmonics (ϕ_n).

The core-probe static and total pressures were used to calculate velocity perturbations in the core flow, which were also Fourier-decomposed in the form of Eq. (1). The coefficients U_n are computed with the equations of the Appendix.

Test Parameters

Test conditions were set by controlling the plenum chamber pressure to achieve a desired ratio of inlet-total to exit-station

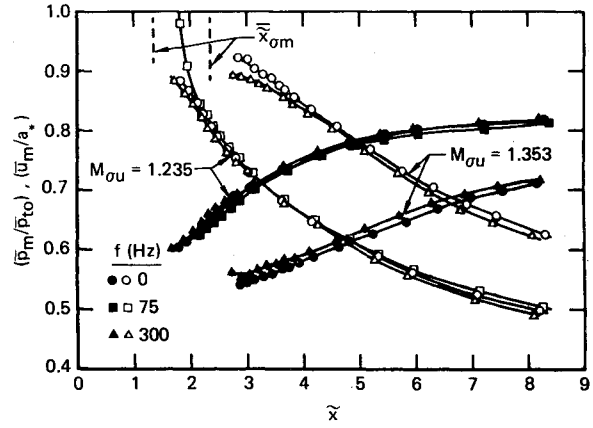

Fig. 5 Streamwise distribution of time-mean core flow pressure (closed symbols) and velocity (open symbols) for different shock strengths and frequencies.

static pressures ($\nu_e \equiv p_{t0}/p_{se}$). This pressure ratio could be controlled and measured precisely and remained temporally constant despite oscillations in the subsonic flow.

Earlier studies showed that the parameter most closely linked with the character of the flow is the Mach number immediately upstream of the shock, at the edge of the top-wall boundary layer ($M_{\sigma u}$). $M_{\sigma u}$ controls the pressure increase imposed by the shock on the boundary layer, determines whether separation will occur, and controls the characteristics of the shock/boundary-layer interaction region, which dominates the overall behavior of the entire flowfield. $M_{\sigma u}$, calculated from the ratio of the minimum top-wall static pressure (occurring just before the shock) and the plenum chamber total pressure, ranged up to 1.353 during these tests. $M_{\sigma u}$ uniquely describes specific flowfield features (such as the occurrence of separation) for all diffusers investigated in this and earlier studies[6-8]; however, the relation between $M_{\sigma u}$ and ν_e is specific to a given diffuser, depending mostly on the area ratio. The $M_{\sigma u}$ (ν_e) relation is monotonic in all cases, and the two quantities can be used interchangeably to characterize the flow.[11]

Control of the pressure ratios implies a concurrent control of Mach number distributions in the flow. Supply-air temperature variations (not controlled) introduced minor variations in the absolute velocities. Reynolds numbers (based on throat height and mean flow conditions at the throat) varied from 0.72 to 0.93×10^6, depending on the pressure/temperature combination in the plenum chamber.

The excitation frequency f and the shock Mach number $M_{\sigma u}$ always describe time-mean test conditions; therefore, overbars will be omitted for simplicity.

Time-Mean Flow and Natural Fluctuations

The character of the flow depends primarily on the shock strength $M_{\sigma u}$. For $M_{\sigma u}<1.27$ (weak shocks), the boundary layers are attached everywhere on both top and bottom walls, and the shock is nearly flat and normal to the flow. Boundary-layer growth is moderate, and merger of the two layers occurs at $\bar{x}\simeq16$-18, well beyond the end of the divergent section. For $M_{\sigma u}>1.28$ (strong shocks), the top-wall boundary layer separates at the foot of the shock, while the bottom-wall boundary layer remains attached. The shock becomes curved, and its shape approximates a lambda pattern. The top-wall boundary layer contains a separation bubble four throat-heights long, and the rate of top-wall boundary-layer growth becomes extremely large. The growth of the bottom layer is suppressed by the rapid thickening of the top layer, but the combined growth is still fast enough to merge the two layers near the end of the divergent channel segment at $\bar{x}\simeq5$-6. In the narrow Mach number range bet-

ween the attached and shock-induced separation ($1.27 < M_{ou} < 1.28$), the flow randomly alternates between these two modes, with abrupt transitions occurring several times per second.

The flow displays natural fluctuations at all flow conditions. Most of the wall pressure fluctuations are associated with local boundary-layer turbulence, covering a broad frequency range that, at most locations, extends above 10 kHz. There also are low-frequency (<300 Hz) oscillations present which are correlated over all of the subsonic flow. Although the contribution of these low frequencies to the total fluctuation energy is small at most locations, the shock responds only to these frequencies; shock displacement spectra contain no contributions over 300 Hz.

Shock displacement spectra show two well-defined peaks (natural frequencies) in the weak-shock case and only one in the strong-shock case (Fig. 4). As discussed in Ref. 11, the natural frequencies in the weak-shock case are well explained by acoustic-wave propagation in both directions, provided the x dependence of the mean flow is taken into account and the shock is assumed to reflect the waves according to Ref. 5. By attaching additional duct segments to the model, it was established that for weak shocks, the frequencies scale inversely with the geometric diffuser length from the shock to the exhaust.

Natural frequencies in the strong-shock case were found to be independent of the geometric length. They scale inversely with the length of the core flow, i.e., with the distance between the mean-shock position and the point where the two wall boundary layers merge. The frequency is closely related to the convection time of pressure perturbations across the core flow region. This case is more complex and less well understood than the weak-shock flows.

Forced Oscillations

Detailed shock motion and unsteady top-wall pressure data were obtained for two selected shock strengths corresponding to attached and separated boundary layers. Figure 4 illustrates how these choices relate to the natural frequencies of the model. For certain selected frequencies, detailed streamwise surveys of mean and fluctuating core pressures (both static and total) were made using the core probe. As an attempt to determine the existence of resonant behavior, the selected frequencies lie either at, or far from, the natural frequencies of Fig. 4.

Figure 5 illustrates that the distributions of the core static pressures and the time-mean core velocities were not appreciably influenced by the periodic perturbations. Figure 5 also shows that the core flow speeds are higher in the strong-shock case, contrary to inviscid predictions. The high speed is caused by the much greater boundary-layer displacement thickness in the strong-shock case,[11] resulting in an equivalent reduction of the effective cross-sectional area.

As mentioned earlier, the exit station pressures serve as reference quantities characterizing the perturbation imposed on the flow, even though the perturbations are generated at the exciter located further downstream. The signals at this location were dominated by the first harmonics at most flow conditions. In general, the contributions from higher harmonics increased with shock strength and frequency. There was no phase shift between the first harmonics from the top and bottom sensors, nor were there any phase differences between transducers on the same wall. This behavior indicates that the wavefront for this component is nearly planar and normal to the flow direction.

Figures 6 and 7 illustrate the excitation-frequency dependence of the exit pressure-fluctuation properties for attached and separated flows. The rms intensities vary between 0.5 and 2.0% of the local static pressure and therefore are relatively small compared with fluctuations observed in ramjet burners, which may reach amplitudes of 20%.

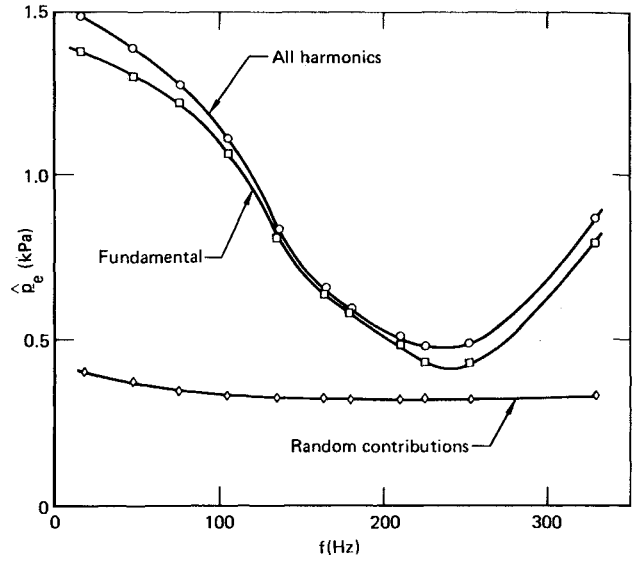

Fig. 6 Wall static pressure perturbation amplitude at the exit as a function of frequency for $M_{ou} = 1.235$.

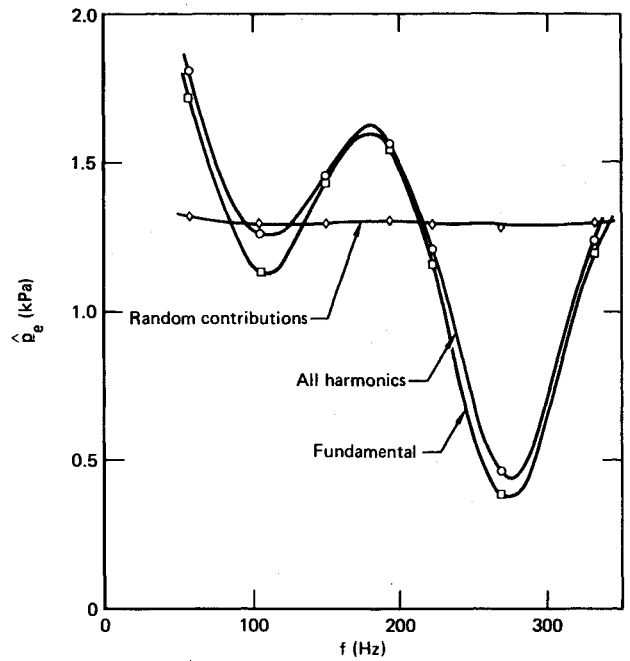

Fig. 7 Wall static pressure perturbation amplitude at the exit station as a function of frequency for $M_{ou} = 1.353$.

The magnitudes of the random contributions are also illustrated in Figs. 6 and 7. The magnitude in each case is independent of frequency, i.e., the cycle-average natural fluctuation intensity is not altered significantly by the imposed perturbations. For weak shocks, the periodic amplitudes dominate; for strong shocks, the periodic and random components are of the same magnitude. Despite the high noise level, the ensemble-averaging and harmonic analysis procedures permitted the determination of important trends and relations.

Time-dependent wall pressure, core pressure, and core velocity perturbations will be presented in the following paragraphs for the dominant first-harmonic contributions in terms of amplitude and phase angle distributions. The amplitudes are one-half of peak-to-peak values, normalized by

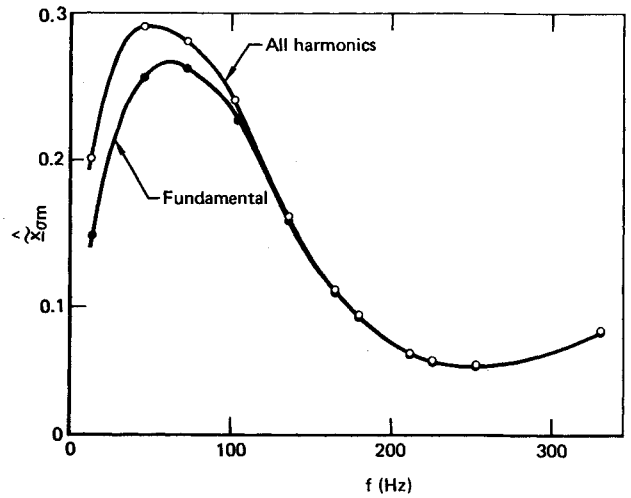

Fig. 8 Shock displacement amplitudes for $M_{\sigma u} = 1.235$.

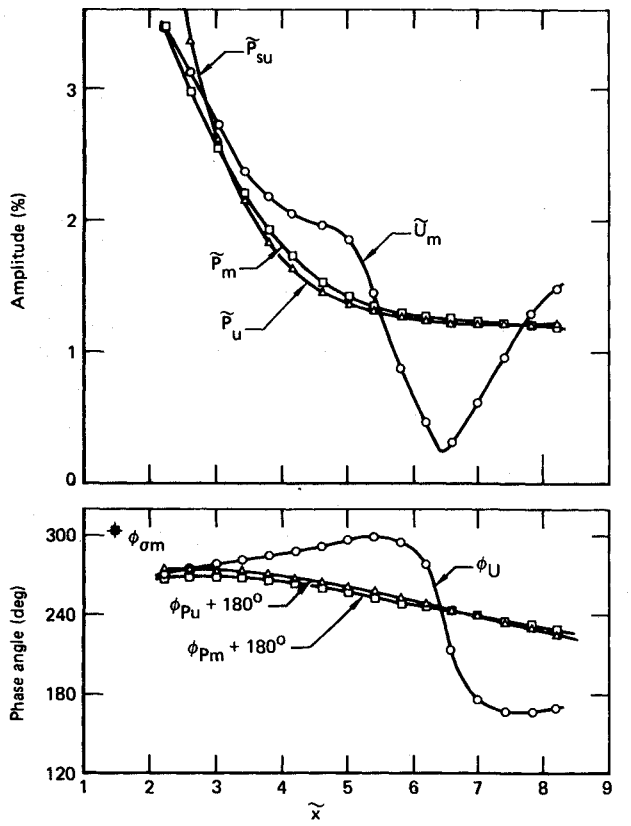

Fig. 9 Streamwise distributions of amplitude and phase angle for the first harmonics of the fluctuations of midstream static pressure, midstream velocity, and upper-wall static pressure. $M_{\sigma u} = 1.235$, $f = 73$ Hz.

local, x-dependent reference quantities. P_{sul} is normalized by $\gamma \bar{p}_{su}$ (from Ref. 11, Fig. 3), P_{sml} by $\gamma \bar{p}_{sm}$ (Fig. 5), and U_{ml} by $\bar{u}_m$ (Fig. 5). Velocities were computed from core-probe data according to expressions given in the Appendix. In the rest of this paper attention will be confined to first harmonics and static pressures; thus, subscripts s and l can be omitted without causing ambiguity.

The instantaneous spatial distributions of the core pressure perturbation can be reconstructed from the data using the expression

$$p'_m(\tilde{x},t) = \gamma \bar{p}_m(\tilde{x})\,\tilde{P}_m(\tilde{x})\cos[2\pi f t - \phi_{Pm}(\tilde{x})] \qquad (2)$$

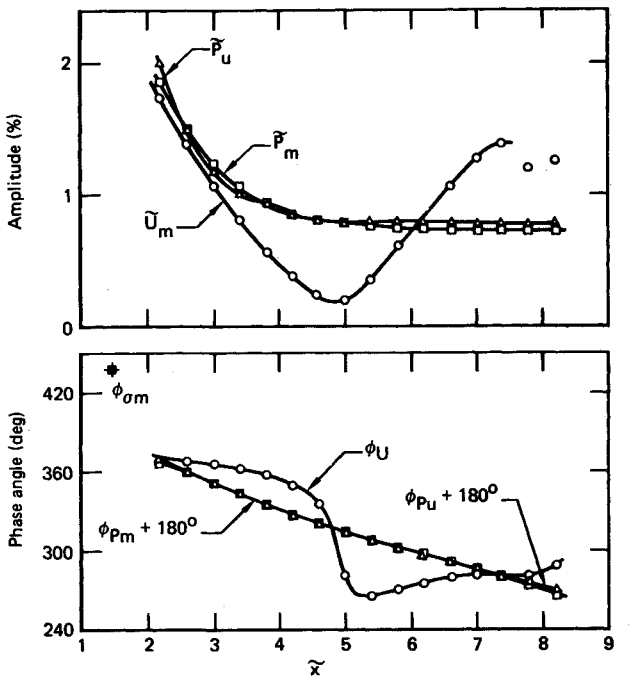

Fig. 10 Streamwise distributions of amplitude and phase angle for the first harmonics of the fluctuations of midstream static pressure, midstream velocity, and upper-wall static pressure. $M_{\sigma u} = 1.235$, $f = 150$ Hz.

Analogous expressions hold for core velocity and wall pressure perturbations.

Equation (2) contains time in the argument of the cosine function only, describing a traveling wave whose speed depends on $\tilde{x}$. For an observer moving with this wave, the argument of the cosine would appear constant, which determines the local wave speed as

$$\left(\frac{d\tilde{x}}{dt}\right)_{[\ ]=\text{const}} = 2\pi f\left(\frac{d\phi_{Pm}}{d\tilde{x}}\right)^{-1} \qquad (3)$$

Thus the speed of the wave is proportional to the inverse slope of the experimental phase angle distribution. It can be shown that propagation speeds deduced from space-time correlations of Eq. (2) are identical to those given by Eq. (3).

Note that the speed obtained from Eq. (3) is associated with the resultant wave which may be composed of two or more contributions. The contributory waves need not move in the same direction as the resultant wave.

Weak Shocks ($M_{\sigma u} = 1.235$)

Figure 8 shows the shock displacement rms values ($\hat{\tilde{x}}_{\sigma m}$) as a function of excitation frequency. The shape of the curve is similar to the $\hat{p}_e(f)$ of Fig. 6, suggesting that the shock displacement amplitudes are proportional to the excitation pressure amplitudes, as expected for small disturbances. However, frequency and amplitude could not be controlled independently (their variation was concurrent according to Fig. 6), and proportionality has not been definitely established.

Figure 8 illustrates that the shock displacement does not become large when the excitation frequency is near either of the known natural frequencies (60 and 230 Hz). This surprising lack of resonant behavior is further confirmed by pressure and velocity data.

The amplitude and phase angle distributions of Figs. 9-11 reveal no significant vertical (transverse) variations in the perturbation pressure field. The streamwise distribution of the pressure perturbation phase angles indicates upstream

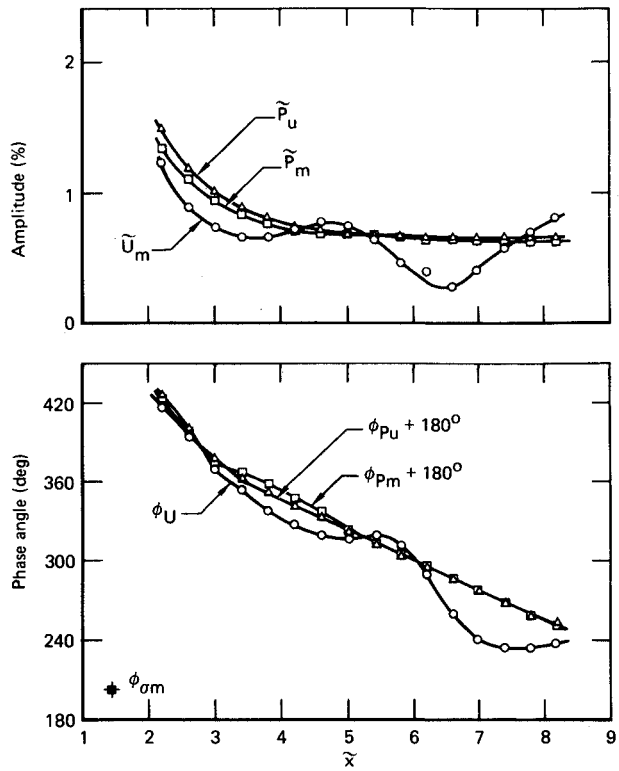

Fig. 11 Streamwise distributions of amplitude and phase angle for the first harmonics of the fluctuations of midstream static pressure, midstream velocity, and upper-wall static pressure. $M_{\sigma u} = 1.235$, $f = 300$ Hz.

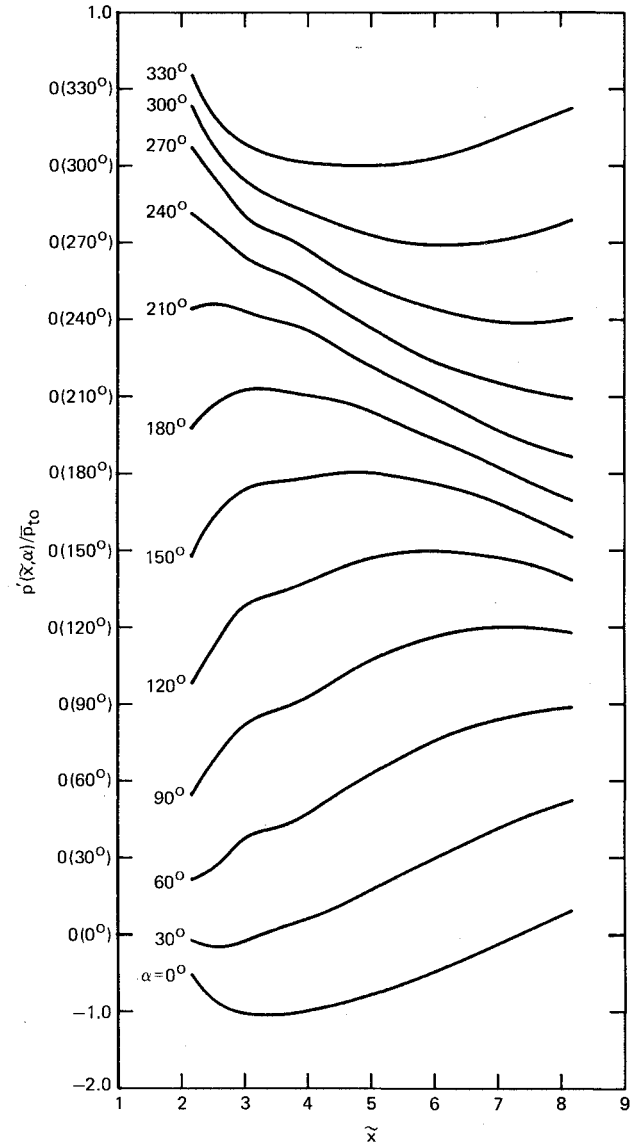

Fig. 12 Streamwise distributions of instantaneous pressure perturbations. $M_{\sigma u} = 1.235$, $f = 300$ Hz.

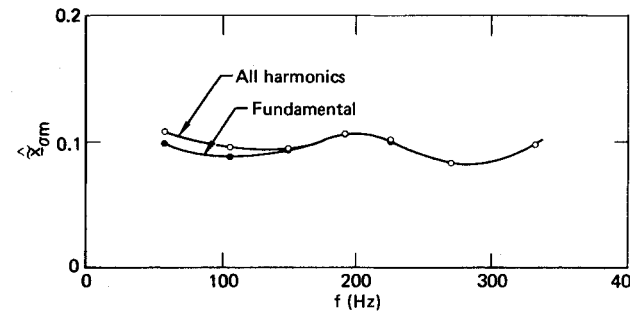

Fig. 13 Shock displacement amplitudes for $M_{\sigma u} = 1.353$.

propagation at speeds from 125 to 230 m/s, with higher excitation frequencies associated with higher speeds. These values are somewhat less than the speed of upstream propagating acoustic waves $(a-u)$, which are computed from time-mean core flow data and stagnation temperature to vary from 120 m/s (at the shock) to 180 m/s (at the exit station), independent of frequency.

Figure 12 shows instantaneous pressure distributions for the 300 Hz case for 30 deg increments of the perturbation phase. The upstream propagation may be seen in the leftward shift of significant features (maximum or minimum). The plot also illustrates that the wavelength is considerably greater than the x range of the measurements.

Pressure perturbation amplitudes show a monotonic increase as the waves propagate upstream and encounter higher mean flow Mach numbers. By the time the wave reaches the shock, the amplitudes are approximately doubled in all three cases. This behavior is consistent with the predictions of transonic, small-disturbance theory applied to diffusers.[9]

The variation of velocity perturbations is more complex; both amplitude and phase angle exhibit local maxima and minima. The number of these extrema increases and the distance between them decreases with increasing excitation frequency, but the decrease is not a simple inverse relation, as might be expected from an acoustic wave pattern. The streamwise distribution of velocity phase angles can be characterized by

$$\phi_U = (\phi_{Pm} + 180 \text{ deg}) + \Delta\phi \qquad (4)$$

i.e., pressure and velocity are 180 deg out of phase, except for small departures, $\Delta\phi$. The departures have a roughly sinusoidal character with amplitudes less than 60 deg and a number of extrema equal to those of the respective amplitude $(\tilde{U}_m)$ distributions. Near the shock, $\Delta\phi \simeq 0$ and the acoustic admittance ratio [Eq. (A8)] is nearly unity for all three frequencies, as expected by the theory of Ref. 5.

Strong Shock ($M_{\sigma u} = 1.353$)

Figure 13 illustrates shock displacement amplitudes as a function of excitation frequency. The amplitudes are smaller than those detected in the weak-shock case and vary only weakly with frequency. The motion is nearly sinusoidal, with only minor higher harmonic content. As was the case with weak shocks, there is no significant evidence of resonant behavior near the natural frequency of 217 Hz.

Figures 14 and 15 illustrate the perturbation fields for two frequencies. The 300 Hz case includes laser velocimeter data

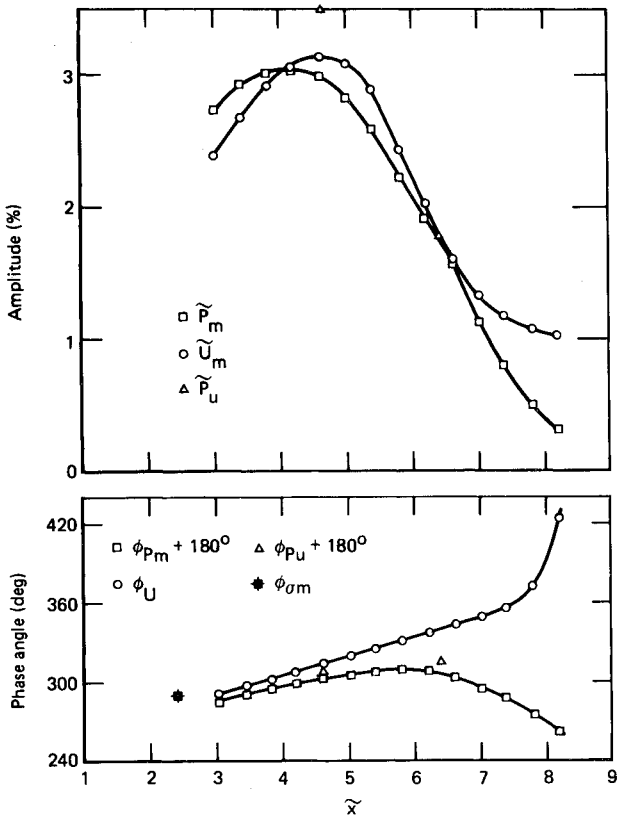

Fig. 14 Streamwise distributions of amplitude and phase angle for the first harmonics of the fluctuations of midstream static pressure, midstream velocity, and upper-wall static pressure. $M_{\sigma u} = 1.353$, $f = 97$ Hz.

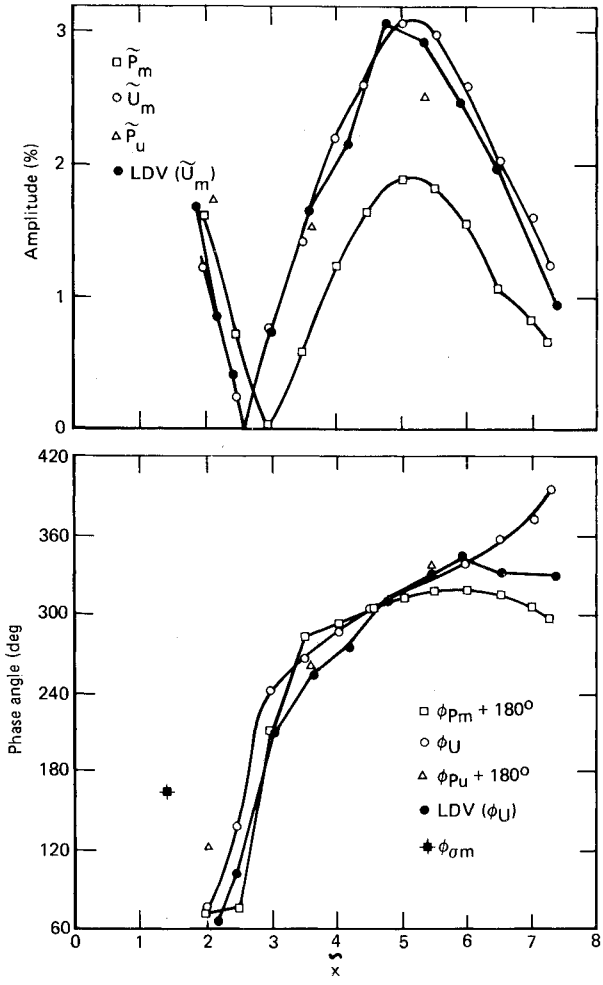

Fig. 15 Streamwise distributions of amplitude and phase angle for the first harmonics of the fluctuations of midstream static pressure, midstream velocity, and upper-wall static pressure. Solid circles are LDV data from Ref. 12. $M_{\sigma u} = 1.353$, $f = 300$ Hz.

taken under the same conditions[12]; the agreement is good, providing credence for data at other conditions.

Comparison of wall and core pressures shows that the pressure fluctuations on the wall are larger, as with natural oscillations.[11] The phase angles in the core and on the wall are virtually identical, again suggesting nearly planar, vertical pressure wavefronts. This result is in sharp contrast with the behavior of phase angles for velocity perturbations, which vary greatly in the vertical direction. The results of Ref. 12 show that velocity phase angles change by 180 deg from the top wall to the midstream position. The vertical distributions of velocity and pressure perturbations thus differ drastically. The distributions of Figs. 14 and 15 also differ substantially from those found in the weak-shock cases. The monotonic variation of pressure amplitude is replaced by distributions displaying a well-defined nodal point and suggesting the presence of another node beyond the $\tilde{x}$ range of the measurements at 300 Hz. The $\tilde{U}_m$ and $\tilde{P}_m$ variations are similar to each other at both frequencies.

Pressure and velocity are out of phase by almost exactly 180 deg at the shock and by approximately the same amount elsewhere. A rapid, 180 deg phase-angle change is observed at the nodal point for both variables.

Figure 16 shows instantaneous pressure distributions for the 300 Hz case. The wavelength is considerably shorter than those found with weak shocks. Downstream propagation is evident from the rightward shift of the maximum from $\tilde{x} = 4$-6, as α changes from 0 to 180 deg. In contrast, the distributions over $4 < \tilde{x} < 7$ exhibit a standing wave, a behavior that is also described by the nearly constant phase angle in this range (Fig. 15).

Discussion

Analysis of the data presented here and in Refs. 11 and 12 shows that a variety of oscillation types may exist depending on the shock Mach number (weak/strong) and on the external perturbations (present/absent). The combinations of these factors largely determine the character of the observed fluctuations and the boundary conditions obeyed by them at the shock.

Boundary Conditions at the Shock

The boundary conditions imposed on the subsonic region determine its possible modes of oscillation. The downstream condition depends on whether excitation is present or not, while the upstream boundary condition is imposed by the shock in all cases.

The reflective properties of a nearly planar shock in a mildly varying area channel are calculated in Ref. 5 using an inviscid, small-perturbation theory. The results indicate a weak reflection (less than 1% for these experiments) and phase shifts between the incident and reflected waves that can vary from 0 to π, depending on frequency and rate of area change.

The experimental results obtained in the present program demonstrate a wide range of responses displayed by the shock, from virtually no reflection to a strong, closed-end-type reflection, depending on the flow conditions, the presence/absence of excitation, and even on the flow property considered. The response will be described here in terms of simple, one-dimensional reflection coefficients, defined as the ratio of the reflected (downstream-moving) and the incident (upstream-moving) perturbations. Both quantities are con-

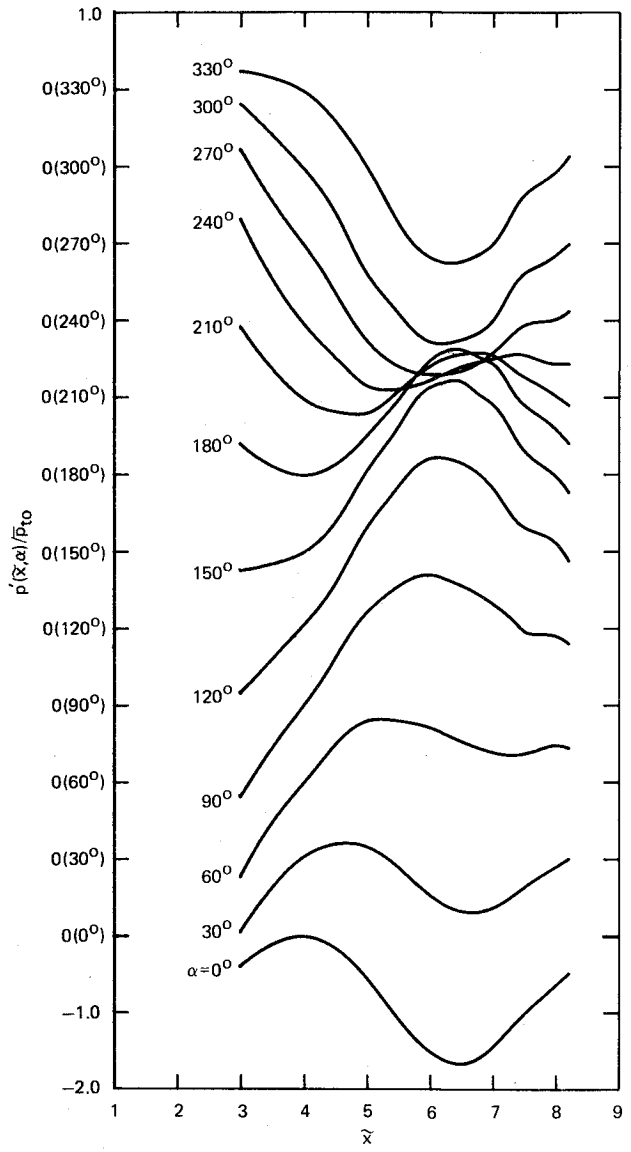

Fig. 16 Streamwise distributions of instantaneous pressure perturbations, $M_{ou} = 1.353, f = 300$ Hz.

sidered as complex so that the reflection coefficient also may be complex ($R = |R|e^{i\psi}$). Table 1 shows inferred reflection coefficients for pressure and velocity, which differ from each other in case of strong shocks. The values of R in the forced-oscillation/weak-shock case was deduced from the $\phi(\tilde{x})$ diagrams (Figs. 9-11), which always indicate up-moving resultant perturbations. Velocity perturbations under the same conditions behave differently; the wavy variation superimposed on the simple upstream propagation trend [described by $\Delta\phi$ in Eq. (4)] is thought to be due to a moderately strong, downstream-moving velocity perturbation reflected from the shock.

Forced-oscillation/strong-shock cases (Figs. 14 and 15) show well-defined nodal points for both pressure and velocity. Nodal points cannot exist unless two wave trains of equal amplitude are present, canceling each other at all times; therefore, the reflection coefficient must be near unity. The reflection coefficient is thought to be complex because the perturbation amplitude near the shock is less than the peak amplitude existing farther downstream, indicating a phase shift at the shock. For a real reflection coefficient with an absolute value of unity, the amplitude at the shock would be a maximum. The physical reason for the phase shift may be a frequency-independent flowtime associated with the readjustment of the boundary layer to a changed core flow condition.

Table 1 Reflection coefficients at shock[a]

Shock strength, M_{ou}	Inferred from data: Natural oscillation	Inferred from data: Forced oscillation
Below 1.27 (Weak shock)	$R_P \ll 1$ $\psi_P \approx 0$-90 deg	$R_P \approx 0$-0.1 $R_U \approx 0.2$-0.5
Above 1.28 (Strong shock)	Not known	$R_P \approx R_U \approx 1$ $\psi_P \approx \psi_U \approx -60$- + 60 deg

[a] P, U = pressure and velocity perturbations, respectively. R = absolute value.

No simple explanation is available for the observed behavior of the reflection coefficients. The one-dimensional model of Ref. 5 is appropriate for pressure perturbations in weak-shock cases, but is inadequate for strong shocks; the actual processes probably depend strongly on boundary-layer effects. Since knowledge of the proper boundary conditions is required to predict diffuser response, clarification of the reflection process at the shock emerges from this study as a key problem demanding further attention.

Character of the Perturbations

Perturbations in the natural-oscillation/weak-shock case are well modeled as one-dimensional acoustic waves; the success of acoustic theory in describing the first three natural frequencies is remarkable.[11]

On the basis of acoustic theory, one expects the reflection coefficients for pressure and velocity perturbations to have the same absolute value. However, the weak-shock case reflection coefficients for velocity perturbations (deduced from forced oscillation data) appear to be greater than those for pressure perturbations under identical circumstances.

In flows with strong shocks, the acoustic approximation is incompatible with the data for both natural and forced oscillations. Natural frequencies do not correlate with acoustic wave propagation times. For forced oscillations, the time-resolved velocity measurements of Ref. 12 illustrate that the velocity-perturbation field is dominated by the transverse-wave motion of the core-flow/boundary-layer interface. The waves travel downstream at a speed less than one-half of the core-flow velocity. The velocity perturbations at the top and bottom walls are out of phase by 180 deg, but the pressure perturbations are not. The transverse waves represent large perturbations of the effective cross-sectional areas of the core flow, and the resultant strong inviscid/viscous interaction is an important characteristic of the perturbation field. Acoustic perturbations must be present, but they are dominated by the large transverse motions.

Because of the complexity of the perturbations in the strong-shock case, their reflection from the shock is also complicated. The reflections involve the classical normal-shock/acoustic-wave interaction in the core flow, but a large part of the reflection is the result of the unsteady modulation of the entire shock/boundary-layer interaction region, and the reflection is determined by properties of the boundary layer as it emerges from an unsteady shock/boundary-layer interaction. It is questionable whether reflection coefficients are adequate for the description of such complex processes. Even if the approximation appears admissible for engineering purposes, separate coefficients are likely to be required for pressure and velocity.

Reference 17 contains extensive discussions of boundary-layer waves, reflections associated with them and calculations of amplitude/phase-angle distributions for simple systems including such waves.

Forced vs Natural Oscillations

The forced oscillation data provide no evidence of resonance-like behavior in any of three candidate conditions

where the natural and excitation frequencies were equal. While a convincing explanation is not available, it is instructive to consider the differences between the two cases.

Earlier studies[8] suggest that low-frequency natural oscillations are excited by turbulence which is most intense in the merger region of the top and bottom boundary layers. In this region the layers are thick, the turbulent structures in them are large, and the frequencies characterizing the local turbulence are low enough to couple with large-scale, coherent modes. This excitation acts in a distributed manner on both walls and along the length of the diffuser. In contrast, the artificial excitation used here is concentrated at one interior location (at the rotor) and in an asymmetric manner (one wall only).

Resonance-like behavior was expected on the basis of one-dimensional, inviscid, acoustic theory which predicts one set of natural modes for a given pair of boundary conditions, regardless of differences in excitation such as those outlined above. In reality, the flow is two-dimensional, which introduces a two-parameter set of natural modes, at least in a purely acoustic situation. The consequences of transverse boundary-layer waves are not fully understood, but they are likely to increase the number of possible oscillatory modes even further.[17]

It is conjectured that the method of excitation used in this work led to oscillation modes different from those occurring under natural (unexcited) conditions. Such a discrepancy would explain why no resonance was found. Substantiation of this conjecture would require time-resolved measurements in a two-dimensional, natural oscillatory flowfield.

These considerations suggest that specific details of excitation may be important in ramjet pressure oscillations. An inlet may be able to tolerate fairly large burner pressure fluctuations as long as they do not excite the natural modes of the inlet. The opposite case of extreme sensitivity, in case of exactly the right type of excitation, is also physically conceivable, although it was not demonstrated in these experiments.

Conclusion

Small-amplitude, periodic oscillations were generated in nominally two-dimensional, supercritical diffuser flows with terminal shock Mach numbers up to 1.35 by modulating the cross-sectional area near the diffuser exhaust at frequencies up to 330 Hz. Detailed measurements of ensemble-averaged shock position histories and static/total pressures in both the interior and on the walls were made.

The pressure fluctuations were generally less than 2% of the local static pressure throughout the diffuser. The amplitude and phase-angle distributions of the imposed pressure and velocity perturbations were calculated from the data for several excitation frequencies, both with and without shock-induced separation.

The results show that neither the mean flow nor the time-mean value of the naturally present fluctuation intensities is altered appreciably by the imposed perturbations. No resonance effects were observed when the excitation frequency was near any of the well-defined natural frequencies determined from shock-displacement spectra.

The character of the forced perturbation field depends on whether the shock is weak (preshock Mach number <1.27, no separation) or strong (Mach number >1.28, shock-induced separation). In the weak-shock case, the pressure perturbations behave as one-dimensional acoustic waves, while the velocity perturbations only approximate such behavior. In the strong-shock case, the perturbations are influenced strongly by interactions between the boundary layer and the core flow, and are not described by one-dimensional acoustic theory.

The interaction of perturbations with the normal shock (reflection) is complex and dependent on shock strength. The findings justify the conclusion that reflection modeling is a key problem in the further development of prediction methods suitable for engineering purposes.

Appendix: Calculation of Velocity Perturbations

The connection between velocity, static pressure, and total pressure in a perfect gas is expressed by the following relation:

$$\left(\frac{u}{a_*}\right)^2 = \frac{\gamma+1}{\gamma-1}\left[1-\left(\frac{p_s}{p_t}\right)^{(\gamma-1)/\gamma}\right] \tag{A1}$$

Assuming that the quasisteady approximation is applicable, differentiating and approximating the small-amplitude perturbations by differentials leads to the formula:

$$\frac{u'}{\bar{a}} = \left[\frac{\gamma-1}{2}\left(\frac{\bar{\mu}}{1-\bar{\mu}}\right)\right]^{1/2}\left(\frac{p_t'}{\gamma\bar{p}_t} - \frac{p_s'}{\gamma\bar{p}_s}\right) \tag{A2}$$

where

$$\bar{\mu} = \left(\frac{\bar{p}_s}{\bar{p}_t}\right)^{(\gamma-1)/\gamma} \tag{A3}$$

Approximating the perturbations of u, p_s, and p_t by the first Fourier harmonic component of each, in the form

$$x' = X_1\cos(2\pi ft - \phi_{X1}) \tag{A4}$$

and introducing the notation

$$\tilde{U}_1 = U_1/\bar{a}, \quad \tilde{P}_{t1} = P_{t1}/\gamma\bar{p}_t, \quad \tilde{P}_{s1} = P_{s1}/\gamma\bar{p}_s \tag{A5}$$

the amplitude and phase of the first harmonic of the velocity fluctuations are

$$\tilde{U}_1 = \sqrt{\frac{\gamma-1}{2}}\sqrt{\frac{\bar{\mu}}{1-\bar{\mu}}}\left[\tilde{P}_{t1}^2 + \tilde{P}_{s1}^2 - 2\tilde{P}_{t1}\tilde{P}_{s1}\cos(\phi_{Pt1} - \phi_{Ps1})\right]^{1/2} \tag{A6}$$

and

$$\cos\phi_{U1} = \sqrt{\frac{\gamma-1}{2}}\sqrt{\frac{\bar{\mu}}{1-\bar{\mu}}}\left(\tilde{P}_{t1}\cos\phi_{Pt1} - \tilde{P}_{s1}\cos\phi_{Ps1}\right)\Big/\tilde{U}_1 \tag{A7}$$

The conventional definition of the acoustic admittance ratio[5] is

$$A \equiv \bar{\rho}\bar{a}(u'/p') \tag{A8}$$

and the admittance for the first harmonic is therefore obtained as

$$A_1 = \tilde{U}_1/\tilde{P}_{s1} \tag{A9}$$

justifying the normalization chosen for the pressure fluctuations in Eq. (A5).

Acknowledgments

This work was sponsored in part by the Air Force Office of Scientific Research under Contract F49720-77-C-0082 and in part by the Independent Research and Development program of McDonnell Douglas Corporation.

References

[1] Rogers, T., "Ramjet Inlet/Combustor Pulsations Study," Naval Weapons Center, China Lake, Calif., NWC TP6053, Jan. 1980.

[2] Rogers, T., "Ramjet Inlet/Combustor Pulsation Analysis," Naval Weapons Center, China Lake, Calif., NWC TP6155, Feb. 1980.

[3]Clark, W. H., "Static and Dynamic Performance Investigations of Side Dump Ramjet Combustors: Test Summary," Naval Weapons Center, China Lake, Calif., NWC 6209, Dec. 1980.
[4]Culick, F.E.C. and Rogers,T., "Modeling Pressure Oscillations in Ramjets," AIAA Paper 80-1192, June 1980.
[5]Culick, F.E.C. and Rogers, T., "The Response of Normal Shocks in Inlet Diffusers," *AIAA Journal*, Vol. 21, Oct. 1983, pp. 1382-1390.
[6]Sajben, M., Kroutil, J. C., Chen, C. P., "A High-Speed Schlieren Investigation of Diffuser Flows with Dynamic Distortion," AIAA Paper 77-875, June 1977.
[7]Sajben, M., Kroutil, J. C., and Chen, C. P., "Unsteady Transonic Flow in a Two-Dimensional Diffuser," *AGARD Conference Proceedings No. 227, Unsteady Aerodynamics*, Sept. 1977, pp. 13-1/13-14.
[8]Sajben, M. and Kroutil, J. C., "Effects of Initial Boundary-Layer Thickness on Transonic Diffuser Flows," *AIAA Journal*, Vol. 19, Nov. 1981, pp. 1386-1393; also, AIAA Paper 80-0347.
[9]Liou, M. S., "Analysis of Viscous-Inviscid Interaction in Transonic Internal Flows," *AIAA Journal*, Vol. 21, July 1983, pp. 963-969.
[10]Coakley, T. J. and Bergmann, M. Y., "Effects of Turbulence Model Selection on the Prediction of Complex Aerodynamic Flows," AIAA Paper 79-0070, Jan. 1979.
[11]Bogar, T. J., Sajben, M., and Kroutil, J. C., "Characteristic Frequencies of Transonic Diffuser Flow Oscillations," *AIAA Journal*, Vol. 21, Sept. 1983, pp. 1232-1240.
[12]Salmon, J. T., Bogar, T. J., and Sajben, M., "Laser Velocimeter Measurements in Unsteady, Separated, Transonic Diffuser Flows," *AIAA Journal*, Vol. 21, Dec. 1983, pp. 1690-1697.
[13]Sajben, M., Bogar, T. J., and Kroutil, J. C., "Forced Oscillation Experiments in Supercritical Diffuser Flows with Application to Ramjet Instabilities," AIAA Paper 81-1487, July 1981.
[14]Sajben, M., Bogar, T. J., Kroutil, J. C., and Salmon, J. T., "Factors Influencing Velocity Distributions at Inlet/Combustor Interfaces," 18th JANNAF Combustion Meeting, Pasadena, Calif., Oct. 1981; CPIA Pub. No. 347, Vol. 3, 1981, pp. 321-331.
[15]Sajben, M. and Crites,R. C., "Real-Time Optical Measurement of Time-Dependent Shock-Position," *AIAA Journal*, Vol. 17, Aug. 1979, pp. 910-912.
[16]Roos, F. W. and Bogar, T. J., "Direct Comparison of Hot-Film Probe and Optical Techniques for Sensing Shock-Wave Motion," *AIAA Journal*, Vol. 20, Aug. 1982, pp. 1071-1076.
[17]Sajben, M. and Bogar, T. J., "Unsteady Transonic Flow in a Two-Dimensional Diffuser: Interpretation of Experimental Results," AFOSR-TR-83-0453, March 1982.